Nonlinear Joint Angle Control for Artificially Stimulated Muscle

Peter H. Veltink, *Member, IEEE,* Howard J. Chizeck, *Member, IEEE,* Patrick E. Crago, *Member, IEEE,* and Ahmed El-Bialy

Abstract—Designs of both open- and closed-loop controllers of electrically stimulated muscle that explicitly depend on a nonlinear mathematical model of muscle input–output properties are presented and evaluated. The muscle model consists of three factors: a *muscle activation dynamics* factor, an *angle-torque relationship* factor, and an *angular velocity torque relationship* factor. These factors are multiplied to relate output torque to input stimulation and joint angle. An experimental method for the determination of the parameters of this model was designed, implemented, and evaluated. An open-loop nonlinear compensator, based upon this model, was tested in an animal model. Its performance in the control of joint angle in the presence of a known load was compared with a PID controller, and with a combination of the PID controller and the nonlinear compensator. The performance of the nonlinear compensator appeared to be strongly dependent on modeling errors. Its performance was roughly equivalent to that of the PID controller alone: somewhat better when the model was accurate, and somewhat worse when it was inaccurate. Combining the nonlinear open loop compensator with the PID feedback controller improved performance when the model was accurate.

INTRODUCTION

IN principle, the contraction of an electrically stimulated muscle can be controlled on the basis of a model of the muscle dynamics. However, although many control strategies for electrically stimulated muscle have been reported in the literature [1]–[10], none have been based on extensive nonlinear muscle models, such as those reported in [11]–[33]. The work reported in this paper is based on the hypothesis that the performance of control strategies can be improved by using more realistic nonlinear models of muscle dynamics. Controllers that are explicitly based upon a nonlinear model of muscle are investigated.

The motivating application of this work is the use of electrical stimulation to restore function of paralyzed limbs. Control of the stimulation has been studied by several authors [1]–[10]. For example, digital fixed parameter PI and PID controllers have been used to obtain robust control of isometric muscle force in animal models [7] and in the human upper [8] and lower [9] extremities. Adaptive controllers based on a linear model of muscle dynamics have also been reported [1], [2]. They did not model the nonlinearities of muscle explicitly, but used linear auto regressive moving average (ARMA) models [34], which were recursively identified. Hausdorff and Durfee reported on the control of knee joint angle of a freely swinging leg, stimulating quadriceps and hamstrings in healthy subjects [35]. They tested an open-loop controller, which compensated for the recruitment characteristics of stimulation and the angle dependence of torque (both nonlinear), and the dynamics of muscle (linear model). They found that taking into account the nonlinearities improved open-loop joint position tracking.

Many muscle models in the literature have been based on the classical work of Hill [11] and Wilkie [12]. These models represent muscle dynamics by a contractile component and nonlinear series and parallel viscoelastic elements [17]–[22]. The force generated by the nonlinear contractile component depends on the neural activation input, and is also length and velocity dependent. Simpler linear dynamic models were found to be sufficient for isometric contraction [25]–[27], or for a specific range of use [23]–[24]. However, Joyce, Rack, and Westbury could only explain their detailed studies of the dynamic behavior of cat soleus muscles under different circumstances [14]–[16] by the model proposed by Huxley [13], [28], which is based on knowledge of the contractile mechanisms of muscle.

The nonlinear model of muscle dynamics used for joint angle control in this study is a modified discrete time version of the Hill model, with the time step equal to the interval between the electrical stimulus pulses. Active muscle force depends on neural activation, muscle length and the velocity of shortening or lengthening [11]–[20]. The model is formulated as a function of joint angle and angular velocity rather than muscle length and velocity. The relations between muscle length and joint angle and between velocity and angular velocity are determined by

the joint angle-dependent moment arm. No series elasticity is incorporated. Therefore, the model consists of a muscle activation factor, an angle-torque factor and an angular velocity-torque factor.

THEORY

A. Model of the Muscle–Skeleton–Load System

We consider the cat's ankle joint, connected to a second order linear external load, as shown in Fig. 1. The joint angle is controlled by stimulation of the sciatic nerve, which innervates the soleus muscle. As a first approximation, the activation dynamics, angle dependence and angular velocity dependence were assumed to be independent. The discrete time model has its time step equal to the stimulus period T_{sp}, which was taken to be constant. The three-factor model is

$$M_{a,k} = A(u_k)f_\varphi(\varphi_k)f_{\dot\varphi}(\dot\varphi_k) \quad (1)$$

$M_{a,k}$ is the torque generated by the muscle contraction; φ_k is the ankle joint angle at time k; $A(u_k)$ is the (normalized) activation dependence; u_k is the input recruitment level (which depends on the stimulus amplitude and pulse width); f_φ is the angle dependence and $f_{\dot\varphi}$ is the (normalized) angular velocity dependence.

A previous study [36] indicated that model (1) can predict the muscle torque with 85–90% accuracy during simultaneous independent pseudorandom variations of recruitment, angle, and angular velocity.

The activation dynamics were assumed to be a linear second-order critically damped system, expressed by

$$A_k = 2aA_{k-1} - a^2A_{k-2} + (1 - 2a + a^2)u_{k-1}. \quad (2)$$

Recruitment input u_{k-1} is determined by the electrical stimulus at time $k - 1$. The steady state value of the normalized activation dynamics equals u. The assumption of critical damping of the activation dynamics is supported by several studies [25]–[27], [37]. Because of this assumption the activation dynamics can be described by the single parameter a.

In this study, recruitment level u was varied through modulation of the width T_{pw} of rectangular cathodic stimulus pulses [38], [39]. The stimulus period T_{sp} was chosen to produce a near fused contraction (100 ms in our study). We define recruitment level u as the isometric steady-state muscle force generated by stimulation at the chosen stimulus period T_{sp}, divided by the maximal isometric steady state muscle force at that T_{sp}. Therefore, $0 \le u \le 1$. We call the relation between T_{pw} and u the recruitment curve R_c, which is a monotonically inreasing nonlinear relation with a threshold and saturation:

$$u = R_c(T_{pw}). \quad (3)$$

The functions f_φ and $f_{\dot\varphi}$ were approximated by linear interpolation between a limited number of measurement points. The angular velocity $\dot\varphi_k$ at time step k was approx-
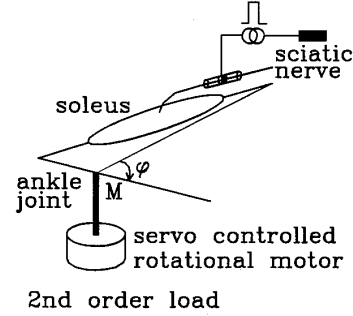

Fig. 1. Schematic representation of the ankle joint of a cat connected to an external load, with stimulation of the soleus muscle. Angle φ and torque M are defined in this figure.

imated from the joint angle at moments k and $k - 1$:

$$\dot\varphi_k \simeq \frac{\varphi_k - \varphi_{k-1}}{T_{sp}}. \quad (4)$$

In the isometric case ($\dot\varphi = 0$) the model (1), (2) is the second order linear discrete time model of muscle dynamics described in [25]. The torque-angle and torque-angular velocity functions have been described in the literature as part of the contractile component of the Hill model (e.g., [11]–[20]).

Fig. 2 is a schematic of the total model of muscle dynamics and load. The torque on the load, M, is balanced by the torque M_a actively generated by the stimulated muscle (1), and by the passive torque M_p, contributed by passive elastic properties of soleus, unstimulated muscles and other passive tissues of the cat's ankle joint:

$$M_k = M_{a,k} + M_{p,k}. \quad (5)$$

The passive torque was modeled as a linear compliance C_p and an offset torque M_{p0} for $\varphi = 0$:

$$M_{p,k} = M_{p0} - \varphi_k/C_p. \quad (6)$$

The external load, which was a second-order linear system in this study, determines the relation between torque and angle:

$$M = I\ddot\varphi + B\dot\varphi + \frac{\varphi - \varphi_{nom}}{C}. \quad (7)$$

Here I is the inertia, B the damping, and C the compliance of the load. These parameters determine the natural frequency f_n and damping ratio ζ of the load [40]. The nominal angle φ_{nom} is the angle at which the steady state torque equals zero. For the controllers, a discrete time approximation (ARMA-model: [34]) of the load was used:

$$\varphi_k = l_1\varphi_{k-1} + l_2\varphi_{k-2} + l_3M_{k-1}$$
$$+ (1 - l_1 - l_2)\varphi_{nom} \quad (8)$$

The discrete time load parameters l_1, l_2, and l_3 were obtained from a continuous time description of the load by an impulse response invariant transformation [40]. The
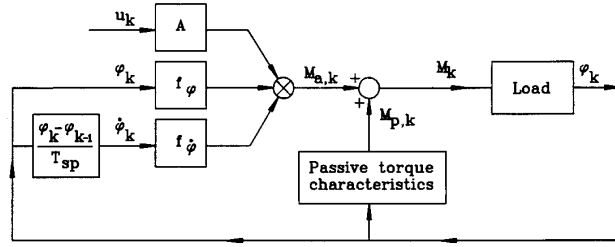
Fig. 2. Total model of muscle dynamics and load. The muscle dynamics
are described by a three-factor model [see (1)] and a linear model of the
passive torque characteristics [see (6)].

torque signal M was integrated by Euler integration (M is assumed to be constant between stimulus pulses).

B. Design of the Control Strategies

The Nonlinear Open-Loop Compensator: An open-loop nonlinear controller can be derived by inversion of the muscle-load model (1)-(6), (8), and substitution of the angle φ_k by the reference angle input $\varphi_{r,k}$. This results in

$$u_k = \frac{A_{k+1} - 2aA_k + a^2 A_{k-1}}{1 - 2a + a^2} \qquad (9)$$

with

$$A_i = \frac{M_{r,i} - M_{p,i}}{f_\varphi(\varphi_{r,i}) f_{\dot\varphi}(\dot\varphi_{r,i})} \qquad i = k - 1, k, k + 1 \qquad (10)$$

and

$$M_{r,i} = \frac{\varphi_{r,i+1} - l_1 \varphi_{r,i} - l_2 \varphi_{r,i-1} - (1 - l_1 - l_2)\varphi_{nom}}{l_3} \qquad (11)$$

$$M_{p,i} = M_{p0} - \frac{\varphi_{r,i}}{C_p}. \qquad (12)$$

The pulse width T_{pwk} can be determined from the required recruitment level u_k using the inverse of the monotonically increasing recruitment curve (3):

$$T_{pwk} = R_c^{-1}(u_k). \qquad (13)$$

The resulting compensation block can be used in series with the actual system (Fig. 3) to create an overall linear (zero-order) system. Note that there is a two time steps delay between the reference signal $\varphi_{r,k}$ and the actual angle $\varphi_{r,k}$ when the reference angle is not known ahead of time. However, when the reference angle is known at least two time steps ahead of time, the compensation can be done without a time delay.

The PID Controller: The performance of the open-loop nonlinear compensator was compared to the performance of a PID controller (Fig. 4). In discrete time the PID controller can be described by a second order difference equa-
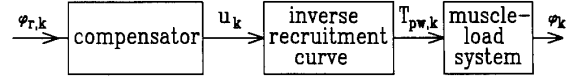

Fig. 3. Block diagram of the open loop nonlinear compensator for control of joint angle. The recruitment level u_k at each time step k is determined from the reference angle φ_{rk} via the nonlinear compensator, which consists of the inverse of the model of the muscle-load system. The recruitment level is transformed to a stimulation pulse width T_{pwk} via the inverse of the recruitment curve.
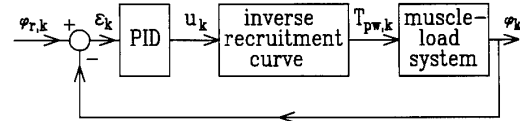

Fig. 4. The PID feedback controller. The error ϵ_k between the reference angle φ_{rk} and the actual angle φ_k is the input of the controller. The output is the recruitment level at each time step k, which is transformed to a stimulation pulse width T_{pwk} via the inverse recruitment curve.

tion [41]:

$$u_k = u_{k-1} + K(\epsilon_k - (z_1 + z_2)\epsilon_{k-1} + z_1 z_2 \epsilon_{k-2}) \qquad (14)$$

where ϵ_k is the difference between the reference angle $\varphi_{r,k}$ and the actual angle φ_k; z_1 and z_2 are the zeros of the PID controller; K is the gain. The recruitment u at time-step k, as calculated by the PID controller, depends on the previous recruitment value, and on the current and two previous error values. In the z-domain, the PID controller is given by the following transfer function [41]:

$$PID\ (z) = \frac{u(z)}{\epsilon(z)} = \frac{K(z - z_1)(z - z_2)}{z(z - 1)}. \qquad (15)$$

For linear systems, the gains, poles, and zeros of the system and controller determine the response characteristics of the closed-loop system [41]. We chose the two zeros of the controller (z_1 and z_2) inside the unit circle at the two outmost pole positions of the (approximate) linear activation dynamics and load models [(2) and (8)]. For a truly linear system, this pole-zero cancellation would result in a relatively fast response (Root Locus Analysis [41]). The gain K was experimentally adjusted on the basis of the overshoot in the response to a step input signal. A small step of $5°$ was used in order to prevent saturation of recruitment. The overshoot was adjusted to a value between 15 and 25%.
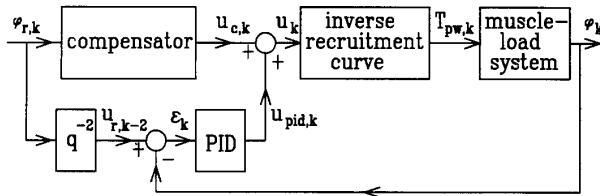
Fig. 5. Combined controller consisting of the open-loop nonlinear compensator and the feedback PID controller. The PID controller was added to compensate for remaining model errors.

Combination of the Nonlinear Compensator and the PID Controller: The third controller considered is a combination of the nonlinear open-loop compensator and the PID controller (Fig. 5). The closed-loop PID controller was added to the nonlinear compensator in order to compensate for model errors and external disturbances not removed by the inversion. The gain K of the PID controller was set at a lower value than for the PID controller alone, in order to favor the integrative part of the controller. An overshoot of less than 15% was experimentally sought during tuning of only the PID controller part.

METHODS

A. Experimental Method

System identification and control strategies were tested in seven acute cat experiments. The first three experiments were used to develop the strategies for identification and control. The last four experiments concentrated on the evaluation of these strategies. Anesthesia was induced with Ketamine initially (30 mg per kg body mass) and was maintained by intravenous injections of sodium pentobarbitol. The initial dose of sodium pentobarbitol was 10 mg per kg body mass. Subsequent doses were titrated to get adequate depth of anesthesia, which was judged on the basis of the absence of reflex withdrawal in response to squeezing the opposite paw and the absence of the eye blink reflex. Atropine was given prior to anesthesia (0.044 mg per kg body mass) to reduce salivation. After 6 h a second injection was given at half the initial dose.

The soleus muscle was stimulated via the sciatic nerve using a monopolar spiral cuff electrode [42]. The cuff electrode was placed around the sciatic nerve at the level of the sciatic notch near the hip of the cat, before the tibial and peroneal nerves branch. A hypodermic needle inserted under the skin in the back of the cat served as the reference electrode. Branches of the sciatic nerve to other muscles were cut, and the sciatic nerve was crushed proximally to the site of stimulation to prevent reflex activation.

The distal tendons of the medial gastrocnemius and plantaris muscles, and other connective tissue, were cut to reduce the passive torque at the ankle. The leg was then closed and sutured, both at the muscle site and at the site of the stimulation electrode.
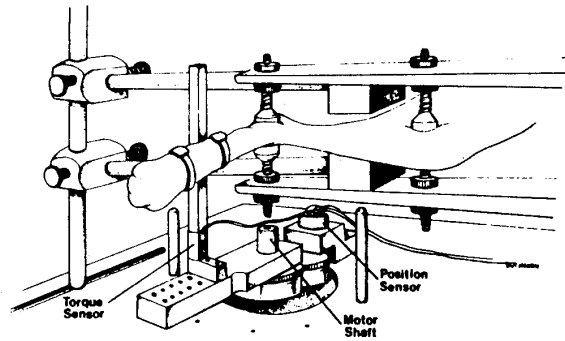

Fig. 6. Cat hind limb mounted in the rotary motor frame. Output torque is measured by semiconductor strain gauges on the cantilever beam. The ankle angle corresponds to the shaft angle of the motor, which is measured using a potentiometer (from reference [2]).

During the experiment the cat lay on a heating pad. A heating lamp was used to maintain (by manual adjustment) the temperature in the hind limb near 34°C. Muscle temperature was monitored by a temperature sensor implanted near the soleus.

The stimulus pulses were mono phasic [39]. The stimulus period T_{sp} was constant at 100 ms. Recruitment u_k at every stimulus period T_{sp} was modulated by varying the pulse width T_{pw} in the range of 50–200 μs. The pulse amplitude had a constant value between 300 and 400 μA.

The cat's paw was connected to a servo controlled rotational motor system (as in [2]). The cat's hind limb was clamped at the ankle and knee joints. The foot was strapped to a cantilever beam equipped with semiconductor strain gauges, measuring angle joint torque (Fig. 6). The shaft angle, corresponding to the ankle joint angle, was measured by a potentiometer. The rotary motor was controlled by a servo with feedback from angle, velocity, and torque sensors (bandwidth about 25 Hz). A second-order linear load was implemented by real-time computation of the desired angle from the torque signal, and setting this angle via the servo system (as was described in [43] for a linear motor system). The load model was computed in real time (100 times per second), in parallel with the program controlling the experiment on a PDP 11/73 computer. The angle computed by the load model was transferred to the reference angle input of the servo control system via an analog output of the computer and a fourth-order low pass reconstruction filter with a cutoff frequency of 50 Hz. This filter reconstructed a smooth reference angle signal from the step like analog output signal. The torque signal M was low-pass filtered with a cutoff frequency of 30 Hz, prior to sampling via a 12-bit AD converter. The actual shaft angle, as measured by the potentiometer, was also sampled, but no presampling filter was used, because this signal's bandwidth was small (below 20 Hz). The load implementation appeared to be accurate and stable for the critically and supercritically damped loads used in this study (natural frequency less than 5 Hz).

B. Identification

Before applying the nonlinear compensator, the recruitment curve, the angle dependent function f_φ and the angular velocity dependent function $f_{\dot\varphi}$ were estimated explicitly in the range of operation of the controller:

1) The *isometric recruitment curve* R_c was determined from responses to a constant pulse train ($T_{sp} = 100$ ms). The pulse width T_{pw} was varied, in successive trains of 5 to 7 steps, between threshold and saturation. The ankle joint angle φ was 90°.

2) The *angular range of operation* of the muscle–skeleton–load system was determined from a constant stimulus train response at maximal recruitment ($u = 1$), with the load attached.

3) The *passive compliance* C_p was determined from the average slope of the angle–torque relation during passive 0.5 Hz sinusoidal angle perturbation, in the angular range of operation. The *offset* M_{p0} was determined separately from the rest torque and angle, with the load attached and the muscle not stimulated (in order to minimize the offset of the nonlinear compensator for the rest angle).

The *angle–torque function* f_φ and *the angular velocity–torque function* $f_{\dot\varphi}$ were determined in two ways.

First, the angle–torque and angular velocity–torque relations were determined from isometric and isokinetic trials:

4) *Isometric angle–torque relation*: The maximal active torque was determined from constant stimulation contractions, at six angles over a range of 50°.

5) The *angular velocity–torque function* for shortening muscle (increasing angle) was determined from *isokinetic responses*: after 2 s initial isometric stimulation, the angle was ramped, at constant shortening velocity, over a 40° range (starting at an ankle angle of 85° or 95°). This was repeated for several angular velocities in the range to be used for the evaluation of the control strategies. The passive response to the same shortening ramps was subtracted from these responses. For each ramp the resulting torque was averaged over 10° in the middle of the angle range. The torque values were normalized by the isometric response at maximal recruitment in the middle of the 10° angle range.

Secondly, f_φ and $f_{\dot\varphi}$ were identified from constant stimulation responses with the load attached (in which the angle, angular velocity and activation were varied simultaneously).

6) The *angle–torque function* f_φ was determined from responses to constant stimulus trains at five recruitment levels u', ranging from 0 to 1, with the load attached. The torque and angle signals were averaged over the last 2 s of the 5 s stimulation trains. In the static case, at a recruitment level u, the dy-

namic model (1) reduces to

$$M_{a,k} = u f_\varphi. \qquad (16)$$

The active torques were found by subtracting the modeled passive torque (6). Therefore, in steady state f_φ is given by

$$f_\varphi = \frac{M_k - M_{p,k}}{u}. \qquad (17)$$

7) *The angular velocity–torque function $f_{\dot\varphi}$ for positive $\dot\varphi$* (shortening muscle) was determined from the response at maximal recruitment ($u = 1$). For every stimulus period a value for $f_{\dot\varphi}$ was determined using (1), (5), and (6):

$$f_{\dot\varphi,k}(\dot\varphi_k) = \frac{M_k - M_p(\varphi_k)}{A_k f_\varphi(\varphi_k)} \qquad (18)$$

To be a single-valued function, the relation between $\dot\varphi$ and $f_{\dot\varphi,k}$ should not have hysteresis. Hysteresis effects were fully attributed to the activation dynamics. Therefore, parameter 'a' of the activation dynamics (2) was adjusted until minimal hysteresis in the relation between $\dot\varphi_k$ and $f_{\dot\varphi,k}$ was obtained. We represented the function $f_{\dot\varphi}$ for shortening muscle by a piece wise linear approximation found by linear regression from the sets of points $(\dot\varphi_k, f_{\dot\varphi,k})$.

The second set of angle–torque and angular velocity–torque functions [6) and 7)] were in first instance used in the compensator, because they were identified with the load attached, which corresponded best with the controller tests.

8) For lengthening muscle (decreasing angle φ) $f_{\dot\varphi}$ was taken equal to 1. We did not investigate the angular velocity–torque function for these eccentric contractions, which were relatively brief during the controller tests.

In the above identification steps, the constant stimulus trains lasted 5 or 6 s, and torque and/or angle signals were averaged over the last 2 s of these bursts. A rest period of at least 60 s was used between stimulus trains, and between trials of the controllers. This appeared to be sufficient to prevent fatigue during the course of the experiment.

Each of the four controller evaluation experiments consisted of four or five sequences of trials, starting with an identification sequence and then with tests of the controllers. The sequences were repeated twice for two loads. In most sequences, the system response was quite stable. Only in a few cases, a part of a sequence had to be discarded, because the response of the open-loop compensator had changed markedly, which was checked several times during a sequence.

RESULTS

A. Muscle Model Identification

Table I summarizes the model parameter values obtained from the four experimental trials.

TABLE I
PARAMETER VALUES OF THE FOUR EVALUATED EXPERIMENTS

A: Values of the Applied Load Parameters

Exp. #	# Trials	$C * 10^2 \left[\dfrac{°}{N \cdot m}\right]$	ζ	f_n [Hz]
I	2	2	2	1
	2	1	2	3
II	2	4	2	1
	2	4	2	3
III	3	2	1	1
	1	2	2	4
	1	2	1	3
IV	2	2	2	1
	2	4	2	3
	1	4	2	1

B: Averages and Standard Deviations of Some Identified Parameter Values

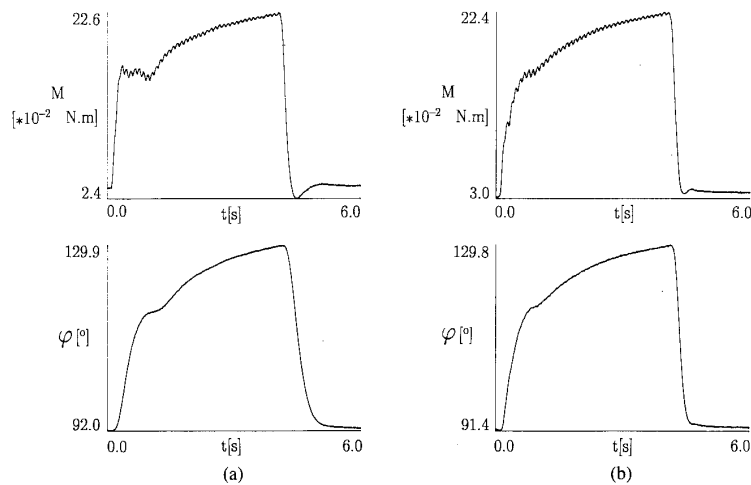| Exp. #	# Trials	$M_{p0} * 10^{-2}$ [N·m]	$C_p * 10^2 \left[\dfrac{°}{N \cdot m}\right]$	f_φ Linearization			f_{an} [Hz]	τ [s]
				h_1	h_2 [s/°]	h_3 [s/°]		
I	4	11 ± 2	6 ± 3	0.78 ± 0.02	0.003 ± 0.003	0.03 ± 0.01	2.4 ± 0.2	—
II	4	2.6 ± 0.5	10 ± 2	0.67 ± 0.06	0.001 ± 0.002	0.03 ± 0.01	2.4 ± 0.1	—
III	5	3.4 ± 0.6	20 ± 8	0.60 ± 0.01	0.000 ± 0.002	0.04 ± 0.01	2.3 ± 0.2	1.09 ± 0.05
IV	5	5.4 ± 0.3	10 ± 3	0.71 ± 0.03	−0.004 ± 0.004	0.05 ± 0.01	3.6 ± 0.7	0.9 ± 0.2

Fig. 7. Two typical examples of burst responses for different loads. The torque registrations are shown in the upper graphs, the angle φ registrations in the bottom graphs: (a) $C = 2.10^2 \; °/N \cdot m$; $\zeta = 1$; $f_n = 1$ Hz. (b) $C = 2.10^2 \; °/N \cdot m$; $\zeta = 1$; $f_n = 3$ Hz.

The Influence of the Load Parameters on Responses to Constant Stimulus Trains: Responses to maximal stimulation bursts were determined for a number of loads, with different compliance, natural frequency f_n and damping ratio ζ (summarized in Table I-A). Two typical responses are shown in Fig. 7.

The nominal angle for the load φ_{nom} (7), (8) was chosen, so that the passive torque was small, and the active torque was high (ankle angle φ between about 85° to 130°). The compliance of the load C was chosen such that an angular excursion of about 35° could be reached by stimulation between zero and full recruitment. The loads were critically or supercritically damped ($\zeta = 1$ or 2) because of limitations in the load implementation. In every experiment, at least two natural frequencies f_n were used, typically 1 and 3 Hz. For lower f_n an overshoot occurred in the torque response while the angular velocity was still low, indicating that the load was slow compared to the

activation dynamics of the muscle. This initial overshoot was followed by a torque decrease during shortening because of the angular velocity dependence, and finally a slow increase to the final torque and angle. For higher f_n the initial overshoot was less or absent because the angular velocity increased quickly.

When stimulation stopped at the end of the burst, active torque fell off very quickly. The following torque overshoot [Fig. 7(a), Fig. 9(c)] cannot be attributed to inertia, because it was less apparent for fast loads [higher f_n, lower ζ: Fig. 7(b)]. It was caused by the angle dependent passive torque.

Recruitment Curve: Fig. 8 shows a sample recruitment curve and the burst responses from which it was determined. The burst responses also illustrate the fusion obtained at a stimulus rate of 10 pulses/s (T_{sp} = 100 ms).

Passive Torque Characteristics: The linear passive model (6) is not very accurate due to nonlinearity, hysteresis, and dependence of the passive properties on the history of stimulation and movement [Fig. 9(a)]. Dependence on movement history is illustrated by the deviating response in the first half cycle of the sinusoidal angle perturbation [Fig. 9(a)]. This illustrates the viscoelastic properties of the muscle. The influence of inertia of the muscle and joint did not appear to contribute greatly to the passive response: increasing the perturbation frequency fourfold (to 2 Hz over a 30° range) did not increase hysteresis and tended to slightly decrease the amplitude of the passive torque response. Dependence on stimulation and movement history is further illustrated by the finding that the passive torque during sinusoidal angle perturbation [Fig. 9(a)] was generally higher than between isometric contractions at different angles [Fig. 9(b), (d)], except for the first half cycle of the sinusoidal perturbation.

The offset M_{p0} of the linear passive model (6) was taken such that the rest angle and torque were the same as between contractions against the load. This minimized the offset of the nonlinear compensator for the rest angle. The passive compliance C_p (6) was derived by linear regression from the average slope of the passive sinusoidal perturbation response. The resulting linear passive angle-torque relation of the model has higher torques in the middle of the angle range than the exponentially shaped angle-torque responses from the sinusoidal perturbation [Fig. 9(a)]. However, at the low and high ends of the range, the error was relatively small. This resulted in low steady-state model errors during the constant parts of the reference inputs of the controllers (Figs. 11 to 14), which were positioned in the low and the high ends of the angle range.

Active Angle-Torque Relation: Fig. 9(d) shows typical active angle-torque relations. These relations were determined from isometric responses at different angles [Fig. 9(b)] and from responses with loads at different recruitment levels [Fig. 9(c)]. Under load (Fig. 9(d), registra-
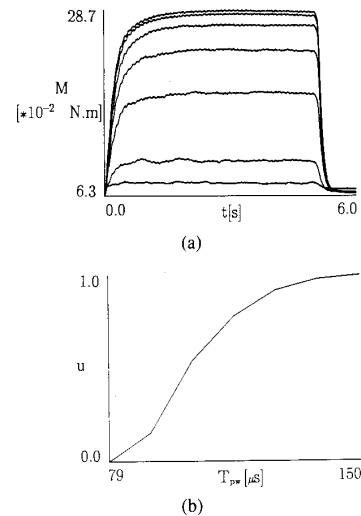

Fig. 8. Typical recruitment curve, determined from isometric burst responses at seven equally spaced pulse widths between threshold and saturation. (a) Isometric constant stimulation responses at 90° ankle angle. (b) Recruitment curve, as determined from these responses.

tions 4 and 6), the torque was lower than in the isometrically measured angle-torque relations (registration 3). This was especially apparent at small angles, at which the errors in passive torque are divided by a small recruitment value u (17). This might in part be due to inaccuracies in the linear passive model (6). The maximal effect was estimated by calculating the angle-torque relation from the responses with load, using the passive angle-torque relation from the isometric angle-torque measurements (Fig. 9(d), registrations 5 and 7). The resulting angle-torque relations are much closer to the isometrically measured angle-torque characteristic (registration 3).

Angular Velocity-Torque Relation

Examples of the angular velocity-torque relations f_φ identified from isokinetic ramp responses and from a burst response with load are displayed in Fig. 10. There are significant differences between them. The shape of the angular velocity-torque relation for positive $\dot\varphi$ (concentric contraction) obtained from the isokinetic ramp trials (registration 1), is similar to those reported by Joyce *et al.* [15] for comparable conditions. As explained, the angular velocity-torque functions used in the nonlinear compensator were obtained from a burst response with load (e.g., Fig. 7), taking into account the passive torque characteristics, the angle-torque relation and the activation dynamics (18). The angular velocity-torque functions obtained in this way can roughly be divided into two linear parts, as is illustrated in Fig. 10. The steep linear part (at low $\dot\varphi$) corresponds to the later part of the burst response (e.g. Fig. 7), where torque and angle gradually approach their
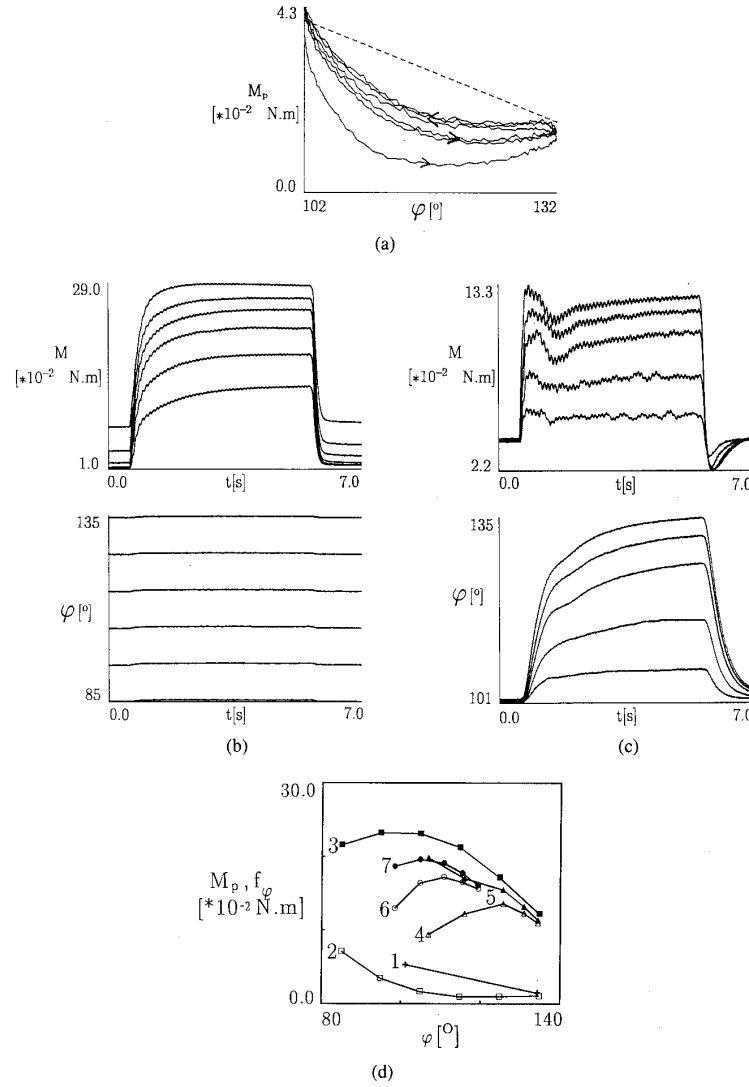
Fig. 9. Passive and active angle–torque relations. (a) Passive angle–torque relation determined from sinusoidal angle perturbations (three periods at a frequency of 0.5 Hz). The estimated linear angle–torque relation is indicated by the dashed line: the linear compliance C_p was determined by linear regression of the response to the second and third period. The offset M_p was determined from angle φ and torque M in rest. (b) Isometric constant stimulation contractions at several angles, from which the isometric angle–torque relation was determined (torque: upper graph, angle: bottom graph). (c) Constant stimulation contractions with load at several recruitment levels. The load characteristics of this example were: $C = 4.10^2 \,°/\text{N} \cdot \text{m}$; $\zeta = 2$; $f_n = 1$ Hz (torque: upper graph, angle: bottom graph). (d) Identification of the angle–torque relations: the relation between angle φ and passive torque M_p: 1) determined from the passive sinusoidal perturbation trial (a). 2) obtained from the isometric trial (b). The relation f_φ between angle φ and active torque M_a: 3) f_φ obtained from isometric constant stimulation responses at full recruitment (b). 4)–7) f_φ obtained from the constant stimulation contractions with load at several recruitment levels [using (17)] [4], 5) load and registrations of (c); 6), 7) other load: $C = 2.10^2 \,°/\text{N} \cdot \text{m}$; $\zeta = 2$; $f_n = 1$ Hz]: 4), 6) f_φ [$M_{p,k}$ determined from sinusoidal contractions: reg. 1]. 5), 7) f_φ [$M_{p,k}$ determined from isometric contractions: reg. 2].

final values. This part intersects with the $\dot{\varphi} = 0$ axis at 1, and its slope is called h_3. The shallow linear part at higher $\dot{\varphi}$ corresponds to the fast changes in torque and angle in the first part of the burst response. It has a small slope h_2 and intersects the $\dot{\varphi} = 0$ axis at a value $h_1(h_1 < 1)$.

Typically, the angular velocity–torque curve from the burst response is multivalued near the point where the two

linear approximations meet. This corresponds to a small temporal decrease of angular velocity, which can also be seen in the burst responses (e.g., Fig. 7).

Activation Dynamics

Average values of the natural frequency f_{an} of the activation dynamics (found by minimizing the angular ve-
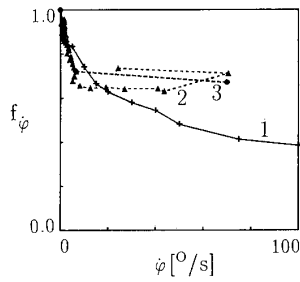
Fig. 10. Angular velocity–torque relations f_φ: 1) From isokinetic ramp responses. 2) Determined from a constant stimulation response at maximal stimulation with attached load (load: $C = 4.10^2$ °/N · m; $\zeta = 2$; $f_n = 3$ Hz). 3) Piece wise linear approximation of registration 2.

locity–torque hysteresis) are listed in Table I-B. They are relatively high compared to values found by Bernotas *et al.* [25] and Baratta *et al.* [26].

B. Controller Performance

Controller strategies were evaluated using a reference signal consisting of two isokinetic ramps, divided by a constant part (Figs. 11–14). Relatively slow ramp velocities were chosen, so that no saturation of recruitment occurred. From an examination of the response of the open-loop nonlinear compensator and from the isokinetically determined velocity–torque function, a modification of the velocity factor f_φ was developed.

The responses of the *open-loop nonlinear compensator* (e.g., Fig. 11) were typically too large during the first ramp (concentric contraction) with a large undershoot in torque when the reference angular velocity $\dot\varphi_r$ goes to zero. The first aspect points to an underestimate of the angular velocity function at the ramp velocity (typically about 10°/s). This is seen systematically at that velocity (Fig. 10). However, increasing the angular velocity function for the ramp velocity (to the value derived in the isokinetic trials) results in a good response to the first ramp, but does not eliminate the undershoot when the velocity goes to zero.

A possible explanation of this undershoot is that it takes some time to generate the maximal torque at zero angular velocity. This can be understood from the sliding filament theory, which is the basis of the Huxley model [13]: it takes some time before the maximal number of bonds at zero velocity have been formed. Joyce *et al.* [15], [16], explained similar observations this way. This means that the slow rise of the torque to its maximum in the burst contractions of Fig. 7, corresponding to the steep part of the angular velocity–torque relation, should be modeled by a dynamic process, and not by an instantaneous angular velocity function.

We modified the angular velocity–torque factor f_φ, describing the steep slope of the angular velocity–torque relation in Fig. 9 by a first order dynamic process with time constant τ, which was identified from the slow rise of the torque response to the maximal torque in the burst re-
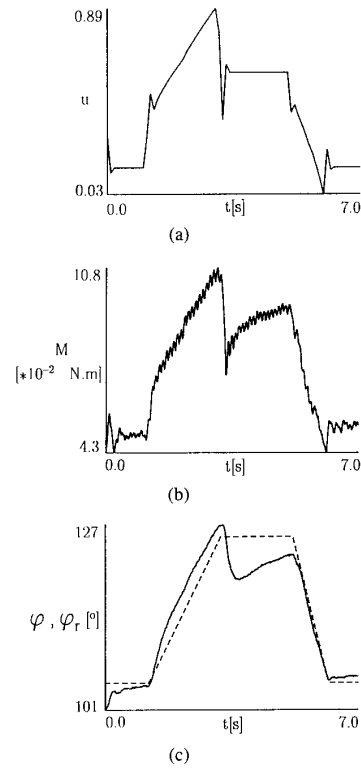

Fig. 11. Typical response of the nonlinear open loop compensator (load: $C = 4.10^2$ °/N · m; $\zeta = 2$; $f_n = 3$ Hz; original f_φ relation); rms-error = 2.7°. (a) Recruitment u. b) Torque M. (c) Actual angle (solid line) and reference angle (dashed line). The reference angle was plotted two time steps delayed.

sponses (Fig. 7):

$$f_\varphi(\dot\varphi) = h_1 - h_2\dot\varphi \quad \text{if } \dot\varphi > \dot\varphi_{\text{thr}}$$

$$= h_1 + \left(1 - \exp\left[-\frac{(t - t_{\text{thr}})}{\tau}\right]\right)(1 - h_1)$$

$$\text{if } 0 < \dot\varphi < \dot\varphi_{\text{thr}} \quad (19)$$

$\dot\varphi_{\text{thr}}$ is the threshold angular velocity between the linear parts of the angular-velocity torque function (Fig. 10), and t_{thr} is the time at which this threshold was reached last.

Increasing f_φ at the ramp velocity to the value obtained from the isokinetic trials, and the addition of the dynamic process for the constant reference angle part, systematically improved the tracking performance of the nonlinear open-loop compensator (Fig. 12; Table II). Note that the recruitment signal gradually decreases in the zero velocity section, instead of remaining constant as in Fig. 11.

The performance of the *PID controller* alone is illustrated in Fig. 13. Changes in the recruitment signal are not as fast as with the nonlinear open-loop compensator, because the PID controller does not incorporate a model of the system. Steady-state errors and ramp tracking appeared to be good, however.

When the model was accurate, a *combination of the PID controller and the nonlinear compensator* improved
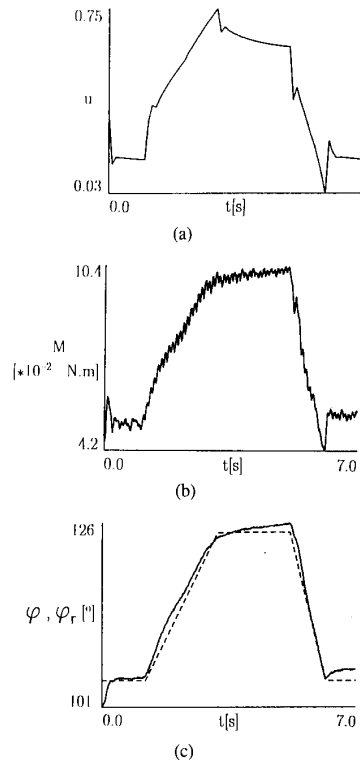
377

Fig. 12. Typical response of the nonlinear open loop compensator with modified f_φ relation (19). Same load as in Fig. 11; (a)-(c): see Fig. 11; rms-error = 1.0°.

TABLE II
AVERAGE VALUES AND STANDARD DEVIATIONS OF THE rms-ERRORS
OF THE CONTROLLERS

		Controller			
		A	B	C	D
Number of trials n		18	10	18	9
Number of experiments		4	2	4	2
rms-error [°]	mean	2.7	1.6	1.5	1.0
	S.D.	1.0	0.8	0.4	0.3

Controller
A   Original nonlinear compensator [original f_φ description].
B   Modified nonlinear compensator [modified f_φ description (19)].
C   PID controller.
D   Combination of modified compensator and PID controller.

tracking performance (Fig. 14; Table II). Fast recruitment changes based on the dynamic model (in the nonlinear compensator) are combined with the capability of the PID feedback controller to obtain the low steady-state errors.

Comparison of the Controller Performances: We evaluated the performance of the control strategies on the basis of the rms errors between the reference angle (delayed two time steps) $\varphi_{r,k-2}$ and the actual angle φ_k for all controller trials (Table II). Performance differences were tested statistically, using the nonparametric sign test [44]
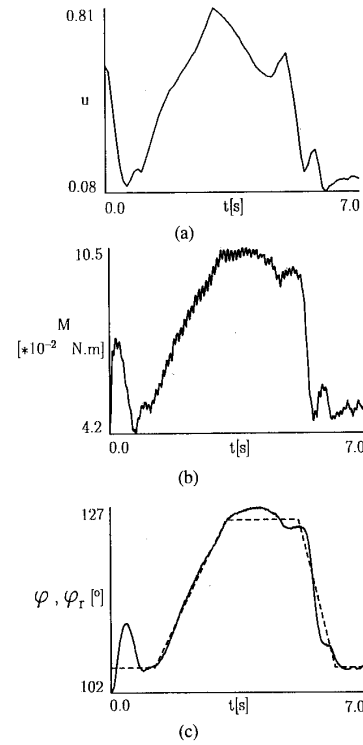

Fig. 13. Typical response of the PID controller. Same load as in Fig. 11; (a)-(c): see Fig. 11; rms-error = 1.7°.
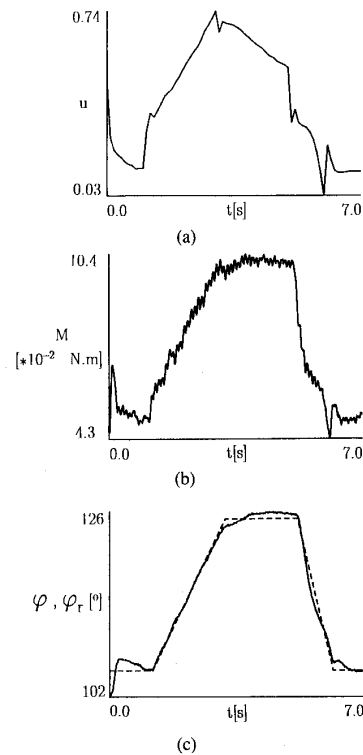

Fig. 14. Typical response of the combined PID controller and nonlinear compensator with modified f_φ relation (19). Same load as in Fig. 11; (a)-(c): see Fig. 11; rms-error = 0.8°.

with significance level $\alpha = 5\%$. The rms errors of the controllers were compared in pairs within each sequence of controller trials. The test was performed over all sequences in the last four experiments. The performance of the compensator with the modified $f_{\dot\varphi}$ was significantly better than the performance of the compensator with the original $f_{\dot\varphi}$ description. Neither the PID controller nor the modified nonlinear compensator was significantly better than the other. The combination of the modified compensator and the PID controller was significantly better than each of them separately.

DISCUSSION

A. The Model of the Muscle–Skeleton–Load System

The three factor structure of the model assumes an independence between A_k, f_φ and $f_{\dot\varphi}$. This is supported by studies of Houk *et al.* [31], [32], who showed that recruitment scaled the length–tension relation of cat soleus in steady state [31] and under dynamic conditions [32]. No clear evidence of the independence between f_φ and $f_{\dot\varphi}$ appears in the literature.

Discarding the series elastic component is justified when this component is stiff compared to the compliance of the load attached to the muscle. Rack and Westbury [33] found that the compliance of the entire tendinous component of the cat soleus varies from 5.10^{-4} m/N at low force to 4.10^{-5} m/N at a high force (11 N). Assuming a moment arm of 10^{-2} m, this results in a compliance of about $2.9 \cdot 10^2$ °/N $\cdot$ m at low torque ($< 10^{-2}$ N $\cdot$ m) to 23 °/N $\cdot$ m at 11.10^{-2} N $\cdot$ m. This indicates that, except for low torques (below 10% of maximal torque), this compliance is low compared to the compliance of the external load (1.10^2 to 4.10^2 °/N $\cdot$ m).

Critically Damped Activation Dynamics: In the isometric case the assumption of critically damped second order linear activation dynamics seems reasonable, considering the findings of [25] and [26]. Baratta *et al.* [26] determined the dynamic responses of soleus at an ankle angle φ of 90°. For several methods of recruitment and firing rate modulation they found that cat soleus muscle behaved as a second-order critically damped system with a natural frequency of 1.85 Hz. Bernotas *et al.* [25] identified a second-order discrete time model of isometric muscle contraction. Using an impulse invariant transformation we calculated that the characteristic frequencies in [25] vary in a wide range (mainly between 1 and 3 Hz), depending on length and stimulus frequency.

A possible explanation of the comparatively high natural frequencies we found (Table I-B) is that the second-order linear model not only describes the actual activation dynamics, but also the effect of the series elasticity in the muscle. This is supported by a study of Bawa *et al.* [27]: the natural frequency of a second-order dynamic model identified at a stimulus rate of 5 or 7 pulses/s was found to be higher in the case of an elastic load (1.4 Hz for a linear compliance equivalent to 1.10^2 °/N $\cdot$ m, assuming

a moment arm of 10^{-2} m) than in the isometric case (0.8 Hz). In addition to the load effect, the estimation of the natural frequency might be influenced by errors in the identification of the passive angle-torque relation.

Linear Passive Angle–Torque Relation: The difference between predicted and actual passive torques in the middle of the angle range was to up about 10% of the maximal active isometric torque. A different description of the passive angle–torque relation (e.g., an exponential relation) might reduce this error. However, there is also a history dependence that can result in errors of the same magnitude as the linear approximation of the passive angle–torque relation.

The Active Angle–Torque Relation f_φ: The active angle–torque relations are similar to length–tension relations, as they are normally presented. Both abscissa and ordinate are influenced by the moment arm, which depends on the joint angle (see [14]).

The differences between the active angle–torque relations found from isometric bursts at several angles and from burst contractions at several recruitment levels when the system was attached to the load can, in part, be explained by the errors in the linear approximation of the passive angle–torque relation. This is especially true at lower recruitment levels because the errors are multiplied by the inverse of the relative recruitment [see (17)].

The Angular Velocity–Torque Relation $f_{\dot\varphi}$: Muscle velocity and joint angular velocity are related by a factor, which is equal to the moment arm (neglecting series elasticity). We did not consider the influence of the joint angle dependence of this moment arm [14].

Part of the observed differences between the angular velocity–torque relations derived from the isokinetic trials, and from constant stimulation contractions with load, may be due to errors in the passive and active angle–torque relations, in the middle of the angle range. These differences might also be due to the limited information used to determine the angular velocity curve from a single constant stimulation contraction. As mentioned earlier, Joyce *et al.* [15], [16] found different angular velocity–torque relations from isokinetic than from isotonic experiments (due to history dependence). They concluded that the Hill model is not adequate to describe muscle dynamics and proposed to use other, Huxley-type models [13]–[16], [28]. The undershoot that we observed in the nonlinear open-loop compensator trials indicates a history dependence for low angular velocity. This is supported by the improvements obtained by the use of the modified nonlinear compensator. It is unlikely that this undershoot is caused by errors in the passive and active angle–torque relations because it occurred at the end of the angle range where both relations have small errors. It is also unlikely that the undershoot was caused by inertia of the muscle-skeleton system because there was no evidence of such inertial influences in sinusoidal passive movements and in response to constant stimulus trains (Fig. 7).

The nonlinear compensators showed good control during the decreasing ramp portions of the reference signal.

The lack of damping during active lengthening thus seems justified in this situation. Further investigation of the model during active lengthening is needed.

B. Control Strategies

It can be concluded that control of joint angle by inversion of a nonlinear dynamic model of the muscle and load is feasible in principle. However, the nonlinear compensator performance compared favorably with a simple PID controller only when it was based on an accurate model of the whole system, including the load. This may limit the use of such controllers to repetitive tasks where loads are well known. Also, only slow, low inertia loads were used, generating relatively slow movements, without saturation of the control input.

In the *control of hand grasp* [8], movements are relatively slow, and muscle contractions can be controlled without saturation. However, loads may be unknown when grasping an object. In such a case, the load must be identified continuously in an adaptive control scheme [1], [2], or the control strategy must be robust to variations in load. Regulation of the stiffness of a joint may be one way to accomplish this, as has been reported in studies of physiological motor control [45]. This principle can also be applied in artificial control using electrical stimulation [8].

In the *control of steady state paraplegic gait* using electrical stimulation [46], the load may be relatively well known [47]. However, saturation of control should be considered because full recruitment stimulation may be required to generate the desired movements of the slow inertial loads, considering the relatively small maximal torques that can be generated by the stimulated muscles [47], [48].

APPENDIX
SYMBOL TABLE

φ	ankle joint angle.
$\dot{\varphi}$	ankle joint angular velocity.
φ_r	reference joint angle.
M	total ankle joint torque.
M_a	active ankle joint torque.
M_p	passive ankle joint torque.
T_{sp}	stimulus period (constant at 100 ms).
T_{pw}	stimulus pulse width.
u	recruitment level (between 0 and 1).
C	Compliance of the load.
I	Inertia of the load.
B	Damping of the load.
f_n	natural frequency of the load.
ζ	damping ratio of the load.
l_1, l_2, l_3	parameters of the discrete time description of the external load (8).
C_p	passive internal load compliance.
M_{p0}	offset passive torque for $\varphi = 0$.
R_c	recruitment curve.
A_k	Activation at time step k.
f_φ	angle–torque relationship.
$f_{\dot{\varphi}}$	angular velocity–torque relationship.

a	parameter of activation dynamics (2).
f_{an}	natural frequency of activation dynamics.
φ_{nom}	nominal angle at which torque exerted by load is zero.
ϵ	error signal (input of the PID controller).
z_1, z_2	zero's of the PID controller.
K	gain of the PID controller.
h_1, h_2, h_3	parameters of f_φ approximation in Fig. 10.
τ	time constant of dynamic process describing development of isometric torque (19).
$\dot{\varphi}_{thr}$	threshold angular velocity between the linear parts of the angular velocity–torque function (19).
t_{thr}	time at which threshold angular velocity $\dot{\varphi}_{thr}$ was last reached (19).

REFERENCES

[1] J. Allin and G. F. Inbar, "FNS control schemes for the upper body," *IEEE Trans. Biomed. Eng.*, vol. 33, pp. 818–828, 1986.

[2] L. A. Bernotas, P. E. Crago, and H. J. Chizeck, "Adaptive control of electrically stimulated muscle," *IEEE Trans. Biomed. Eng.*, vol. 34, pp. 140–147, 1987.

[3] D. K. Peterson and H. J. Chizeck, "Linear quadratic control of a loaded agonist–antagonist muscle pair," *IEEE Trans. on Biomed. Eng.*, vol. 34, pp. 790–796, 1987.

[4] B. H. Zhou, R. Baratta, and M. Solomonow, "Manipulation of muscle force with various firing rate and recruitment control strategies," *IEEE Trans. Biomed. Eng.*, vol. 34, pp. 128–139, 1987.

[5] J. A. van Alsté, P. H. Veltink, and H. Neijmeijer, "Muscle length control by electrical nerve stimulation," in *Proc. 9th IEEE/EMBS Conf.*, Boston, MA, 1987, pp. 1372–1373.

[6] P. H. Veltink and J. A. van Alsté, "Dynamics and control of a muscle-load system during electrical nerve stimulation," *Automedica*, vol. 11, pp. 91–98, 1989.

[7] H. J. Chizeck, P. E. Crago, and L. S. Kofman, "Robust closed-loop control of isometric muscle force using pulse width modulation," *IEEE Trans. Biomed. Eng.*, vol. 35, pp. 510–517, 1988.

[8] P. E. Crago, R. J. Nakai, and H. J. Chizeck, "Feedback regulation of hand grasp opening and contact force during stimulation of paralyzed muscle," *IEEE Trans. Biomed. Eng.*, vol. 38, pp. 17–28, 1991.

[9] J. J. Abbas and H. J. Chizeck, "Feedback control of coronal plane hip angle in paraplegic subjects using functional neuromuscular stimulation," *IEEE Trans. Biomed. Eng.*, vol. 38, pp. 687–698, 1991.

[10] M. N. Oguztöreli and R. B. Stein, "Optimal control of antagonistic muscles," *Biol. Cybern.*, vol. 48, pp. 91–99, 1983.

[11] A. V. Hill, "The heat of shortening and the dynamic constants of muscle," *Proc. R. Soc. London, Ser. B.*, vol. 126, pp. 136–185, 1938.

[12] D. R. Wilkie, "Relation between force and velocity in human muscle," *J. Physiol.*, vol. 110, pp. 249–280, 1950.

[13] A. F. Huxley, "Muscle structure and theories of contraction," *Prog. Biophysics and Biophysical Chem.*, vol. 7, pp. 257–318, 1957.

[14] P. M. H. Rack and D. R. Westbury, "The effect of length and stimulus rate on tension in the isometric cat soleus muscle," *J. Physiol.*, vol. 204, pp. 443–460, 1969.

[15] G. C. Joyce, P. M. H. Rack, and D. R. Westbury, "The mechanical properties of cat soleus muscle during controlled lengthening and shortening movements," *J. Physiol.*, vol. 204, pp. 461–474, 1969.

[16] G. C. Joyce and P. M. H. Rack, "Isotonic lengthening and shortening movements of cat soleus muscle," *J. Physiol.*, vol. 204, pp. 475–491, 1969.

[17] H. Hatze, "A myocybernetic control model of skeletal muscle," *Biol. Cybern.*, vol. 25, pp. 103–119, 1977.

[18] ——, "A general myocybernetic control model of skeletal muscle," *Biol. Cybern.*, vol. 28, pp. 143–157, 1978.

[19] A. L. Hof and J. W. van den Berg, "EMG to force processing I: An electrical analogue of the hill muscle model," *J. Biomech.*, vol. 14, pp. 747–758, 1981.

[20] ——, "EMG to force processing II: Estimation of parameters of the hill muscle model for the human triceps surae by means of a calfergometer," *J. Biomech.*, vol. 14, pp. 759–770, 1981.

[21] J. M. Winters and L. Stark, "Analysis of fundamental human movement patterns through use of in-depth antagonistic muscle models," *IEEE Trans. Biomed. Eng.*, vol. 32, pp. 826–839, 1985.

[22] F. E. Zajac, "Muscle and tendon: Properties, models, scaling, and application to biomechanics and motor control," *CRC Crit. Rev. Biomed. Eng.*, vol. 17, pp. 359–411, 1989.

[23] J. Allin and G. F. Inbar, "FNS parameter selection and upper limb characterization," *IEEE Trans. Biomed. Eng.*, vol. 33, pp. 809–817, 1986.

[24] M. N. Oguztöreli and R. B. Stein, "Analysis of a model for antagonistic muscles," *Biol. Cybern.*, vol. 45, pp. 177–186, 1982.

[25] L. A. Bernotas, P. E. Crago, and H. J. Chizeck, "A discrete-time model of electrically stimulated muscle," *IEEE Trans. Biomed. Eng.*, vol. 33, pp. 829–838, 1986.

[26] R. Baratta, B. H. Zhou, and M. Solomonow, "Frequency response model of skeletal muscle: effect of perturbation level, and control strategy," *Med. Biol. Eng. Comput.*, vol. 27, pp. 337–343, 1989.

[27] P. Bawa, A. Mannard, and R. B. Stein, "Effects of elastic loads in the contractions of cat muscles," *Biol. Cybern.*, vol. 22, pp. 129–137, 1976.

[28] G. I. Zahalak, "A comparison of the mechanical behavior of the cat soleus muscle with a distribution-moment model," *J. Biomech. Eng.*, vol. 108, pp. 131–140, 1986.

[29] I. W. Hunter and M. J. Korenberg, "The identification of nonlinear biological systems," *Biol. Cybern.*, vol. 55, pp. 135–144, 1986.

[30] J. M. Winters and L. Stark, "Muscle models: What is gained and what is lost by varying model complexity," *Biol. Cybern.*, vol. 55, pp. 403–420, 1987.

[31] J. C. Houk, J. J. Singer, and M. R. Goldman, "An evaluation of length and force feedback to soleus muscles of decerebrate cats," *J. Neurophysiol.*, vol. 33, pp. 784–811, 1971.

[32] T. R. Nichols and J. C. Houk, "Improvement in linearity and regulation of stiffness that results from actions of stretch reflex," *J. Neurophysiol.*, vol. 39, pp. 119–142, 1976.

[33] P. M. H. Rack and D. R. Westbury, "Elastic properties of the cat soleus tendon and their functional importance," *J. Physiol.*, vol. 347, pp. 479–495, 1984.

[34] L. Ljung, *System Identification, Theory for the User.* Englewood Cliffs, NJ: Prentice Hall, 1987.

[35] J. M. Hausdorff and W. K. Durfee, "Open-loop position control of the knee joint using electrical stimulation of the quadriceps and hamstrings," *Med. Biol. Eng. Comput.*, vol. 29, pp. 269–280, 1991.

[36] K. Geng, "Real-time parameter identification of a class of nonlinear discrete-time models of electrically stimulated muscle," M.Sc. thesis CWRU, 1989.

[37] W. K. Durfee and K. E. MacLean, "Methods for estimating isometric recruitment curves of electrically stimulated muscle," *IEEE Trans. Biomed. Eng.*, vol. 36, pp. 654–667, 1989.

[38] P. E. Crago, P. H. Peckham, J. T. Mortimer, and J. P. van der Meulen, "The choice of pulse duration for chronic electrical stimulation via surface, nerve and intramuscular electrodes," *Ann. Biomed. Eng.*, vol. 2, pp. 252–264, 1974.

[39] P. H. Gorman and J. T. Mortimer, "The effect of stimulus parameters on the recruitment characteristics of direct nerve stimulation," *IEEE Trans. Biomed. Eng.*, vol. 30, pp. 407–414, 1983.

[40] A. V. Oppenheim, A. S. Willsky, and I. T. Young, *Signals and Systems.* Englewood Cliffs, NJ: Prentice Hall, 1983.

[41] C. L. Phillips and H. T. Nagle, *Digital Control System Analysis and Design.* Englewood Cliffs, NJ: Prentice Hall, 1984.

[42] G. G. Naples, J. T. Mortimer, A. Scheiner, and J. D. Sweeney, "A spiral nerve cuff electrode for peripheral nerve stimulation," *IEEE Trans. Biomed. Eng.*, vol. 35, pp. 905–916, 1988.

[43] P. H. Veltink, J. E. van Dijk, and J. A. van Alsté, "Programmable dynamic muscle load for animal experiments," *Med. Biol. Eng. Comput.*, vol. 26, pp. 234–236, 1988.

[44] J. L. Devors, *Probability and Statistics for Engineering and the Sciences.* Monterey, CA: Brooks/Cole, 1987.

[45] N. Hogan, "Adaptive control of mechanical impedance by coactivation of antagonist muscles," *IEEE Trans. Automat. Contr.*, vol. 29, pp. 681–690, 1984.

[46] H. J. Chizeck, R. Kobetic, E. B. Marsolais, J. J. Abbas, I. H. Donner, and E. Simon, "Control of functional neuromuscular stimulation systems for standing and locomotion in paraplegics," *Proc. IEEE*, vol. 76, pp. 1155–1165, 1988.

[47] G. T. Yamaguchi and F. E. Zajac, "Restoring unassisted natural gait to paraplegics via functional neuromuscular stimulation: A computer stimulation study," *IEEE Trans. Biomed. Eng.*, vol. 37, pp. 886–902, 1990.

[48] P. H. Veltink, "Control of FES-induced cyclical movements of the lower leg," *Med. Biol. Eng. Comput.*, vol. 27, pp. NS8–NS12, 1991.

Peter H. Veltink (S'85–M'88) received the M.Sc. degree in electrical engineering from the University of Twente, Enschede, the Netherlands, in 1984, and the Ph.D. degree in 1988 (topic: recruitment of myelinated nerve fibers during artificial nerve stimulation).

In 1989 he was a visiting assistant professor at Case Western Reserve University, Cleveland, OH, where he did research in the area of nonlinear control of muscle contraction. Currently, he is a faculty member of the Biomedical Engineering Department of the Faculty of Electrical Engineering, University of Twente. His research is in the area of control of functional neuromuscular stimulation, which is carried out in cooperation with the Roessingh Rehabilitation Center in Enschede.

Howard J. Chizeck (S'74–M'79–M'81) was born on March 27, 1952 in Columbus, OH. He received the B.S. and the M.S. degrees in systems and control engineering from Case Western Reserve University in 1974 and 1976, respectively, and the Sc.D. degree in electrical engineering and computer science from the Massachusetts Institute of Technology, Cambridge, in 1982.

He is an Associate Professor in the Systems Engineering and Biomedical Engineering Departments at Case Western Reserve University. His research interests involve applications of control engineering to biomedical problems. Current projects include the design and analysis of controllers for the electrical stimulation of paralyzed muscle, adaptive control of drug delivery, identification and control of cerebral ventricle volume dynamics for hydrocephalus management, algebraic modeling of DNA sequence-geometry relationships and applications of algebraic systems theory to coding.

Dr. Chizeck is a member of AAAS, Sigma Xi, the Rehabilitation Engineering Society of North America (RESNA), and the International Federation of Automatic Control (IFAC) Technical Committee on Biomedical Engineering.

Patrick E. Crago (S'66–M'67–M'86) received the B.S. degree in electrical engineering from Carnegie-Mellon University, Pittsburgh, PA, in 1967, and the M.S. and Ph.D. degrees in biomedical engineering from Case Western Reserve University, Cleveland, OH, in 1970 and 1973, respectively.

He is currently Associate Professor of Biomedical Engineering at Case Western Reserve University. His research interests include the analysis of normal and abnormal neuromuscular control mechanisms, and the restoration of movement by functional neuromuscular stimulation. Current research projects include the development of multiple degree of freedom feedback control systems for regulating limb movement trajectories, the clinical implementation and evaluation of feedback control systems for hand grasp, and the assessment of the effects of electrical stimulation on spasticity in subjects with spinal cord injury.

Ahmed El-Bialy, photograph and biography not available at the time of publication.